2021

Effect Of The Refrigerant Charge On The System Performance And Mass Distribution In Air-To-Water Heat Pumps

Costantino Guzzardi
University of Padova, costantino.guzzardi@phd.unipd.it

Marco Azzolin
University of Padova

Sandro Lazzarato
Clivet S.p.A

Davide Del Col
University of Padova

Effect of the refrigerant charge on the system performance and mass distribution in air-to-water systems

Costantino GUZZARDI[1], Marco AZZOLIN[1], Sandro LAZZARATO[2], Davide DEL COL[1]*

[1]Università degli Studi di Padova, Dipartimento di Ingegneria Industriale,
Via Venezia 1 – 35131, Padova, Italy
costantino.guzzardi@phd.unipd.it
marco.azzolin@unipd.it
davide.delcol@unipd.it

[2]Clivet S.p.A., R&D Department,
Via Camp Lonc 25 - 32030, Villapaiera (BL), Italy
s.lazzarato@clivet.it

* Corresponding Author

ABSTRACT

Recent regulations in the matter of climate change and environmental protection are pushing to reduce the release of greenhouse gases into the atmosphere. The overall environmental impact of a refrigeration system can be reduced by optimizing and possibly minimizing the amount of refrigerant charge in the system. Even in the case of natural and low-GWP synthetic refrigerants, due to the well-known problems with toxicity and flammability, it is required to minimize the amount of refrigerant charged into the system to reduce the associated risks. The charge minimization process requires to know the refrigerant distribution to identify and redesign the critical components in terms of charge retention. This paper analyses numerically the influence of the refrigerant charge on the system performance and on the mass distribution in an air-to-water reversible heat pump working with R32. A mathematical model has been developed to simulate the unit during the cooling mode operation. The model uses the finite volume method to predict the refrigerant charge within the heat exchangers; the amount of refrigerant dissolved in the compressor oil is also accounted for. The results show that most of the charge is stored into the condenser and highlight the existence of an optimum charge that maximizes the system COP. The same model allows to compare various refrigerants in terms of direct and indirect impact on the greenhouse effect.

1. INTRODUCTION

The environmental impact of a refrigeration equipment depends on the refrigerant losses (direct effect) and on the energy consumption (indirect effect) during the whole lifetime of the system. The recent European F-gas regulation (Regulation No 517 of European Union, 2014), in the matter of environmental protection, has introduced a large reduction of the amount of HFC gases to be placed on the European market in the following years. In this scenario, it is important to identify long-term alternatives to the high-GWP refrigerants. Hydrofluoroolefins (HFO) and natural fluids are receiving particular attentions for their low direct environmental impact (zero ODP, low-GWP, short atmospheric lifetime). However, substituting a high-GWP refrigerant with an environmentally friendly one is convenient, from an economical and environmental point of view, only if the system efficiency is not degraded; otherwise the lower direct greenhouse effect could be nullified by a higher electricity demand. In addition, even though these alternatives present low values of GWP, they have problems with toxicity and/or flammability. A way for reducing the risks associated to the use of hazardous fluids is to minimize the amount of refrigerant charged into the system without losing the unit efficiency. The minimization process requires the understanding of the refrigerant distribution among the different components of the system together with a critical review of the role of each component (Corberán, 2010). This paper wants to analyse, numerically, the influence of the refrigerant charge on the system efficiency and on the mass distribution among the components of the equipment. A simulation tool has been developed to predict the refrigerant distribution in air-to-water systems; the model has been validated by testing a commercialized heat pump during the cooling mode operations and it has been used to compare various refrigerants in terms of direct and indirect greenhouse effect.

2. MODEL DESCRIPTION

A mathematical model, named *Charge Calculator*, has been developed in order to calculate the refrigerant charge in air-to-water systems and predict its distribution among the components. The software has been developed in the Matlab environment. The simulation tool is composed by four sub-models, which simulate the main components of the system, i.e. compressor, condenser, expansion valve and evaporator; other components (such as pipelines, receivers, filters, etc.) can be also added to the model. The total refrigerant charge is calculated by adding up the contribution of all the components included in the simulation.

2.1 Compressor model

Compressor is simulated using the performance curves provided by the manufacturer. The compressor model receives as input the refrigerant saturation temperatures at inlet and outlet, the compressor frequency and the degree of vapor superheating at the compressor inlet. The model outputs are: the refrigerant mass flow rate, the compressor power and the gas temperature at the compressor outlet. The refrigerant mass in the compressor is calculated with equation (1):

$$M = \rho \cdot V + \left(\frac{\xi}{1-\xi}\right) \cdot M_{oil} \tag{1}$$

The term $\rho \cdot V$ represents the mass of vapor refrigerant in the compressor shell; the second term represents the refrigerant mass dissolved in lubricant oil. The density of the superheated vapor ρ is calculated from the suction pressure and temperature using Refprop 9.1 (Lemmon *et al.*, 2013); the volume of the component V, and the mass of oil charged in the system M_{oil} are provided as input. The refrigerant solubility in oil ξ is estimated using the oil-refrigerant solubility curves as a function of the suction pressure and oil temperature; the oil temperature is calculated with the correlation proposed by Navarro *et al.* (2012).

2.2 Heat exchanger models

Charge Calculator can simulate various type of heat exchangers when working as condenser or evaporator. Here the model is presented considering an air-to-water heat pump when working as a chiller: the condenser is a fin-and-coil heat exchanger and the evaporator is a brazed plate heat exchanger. To improve the accuracy of the calculation, the heat exchangers are discretized into small finite elements; for each element, a mass and energy balance allows to calculate the outlet conditions of the two fluids. The actual heat flow rate exchanged by the fluids is evaluated using the e-NTU method, considering a cross-flow configuration for the fin-and-coil heat exchanger and a counter-flow configuration for the brazed plate heat exchanger. The correlations used to calculate heat transfer coefficients and pressure drops are listed in Table 1. The heat exchanger models require as input the mass flow rates, the inlet thermodynamic state of the fluids and the condenser subcooling or the evaporator superheating. By applying the secant method, the model calculates iteratively the condensation or the evaporation temperature, which guarantees the refrigerant subcooling or superheating set as input.

The refrigerant mass, in each element, is calculated with equation (2) if the refrigerant is single-phase or with equation (3) if it is two-phase.

$$M = \rho \cdot V \tag{2}$$

$$M = [\alpha \cdot \rho_v + (1-\alpha) \cdot \rho_l] \cdot V \tag{3}$$

V is the volume of the element, ρ is the density of the single-phase refrigerant, ρ_v and ρ_l are respectively the saturated vapor and liquid density of the refrigerant and α is the void fraction. The refrigerant void fraction is calculated with the Taitel and Barnea (1990) correlation for the fin-and-coil heat exchanger (condenser) and with the Baroczy (1963) correlation for the brazed plate heat exchanger (evaporator). Once all the finite elements have been solved, the total charge is obtained by adding up the contribution of each element.

Table 1: Correlations for heat transfer coefficients HTC and pressure drops ΔP in the condenser and evaporator models.

	CONDENSER MODEL		**EVAPORATOR MODEL**	
	HTC	**ΔP**	**HTC**	**ΔP**
Air	Abu Madi *et al.* (1998)	Abu Madi *et al.* (1998)	-	-
Single-phase refrigerant	Ravigururajan and Bergles (1996)	Li *et al.* (2012)	Martin (1996)	Martin (1996)
Two-phase refrigerant	Cavallini *et al.* (2009)	Cavallini *et al.* (2009)	Amalfi *et al.* (2016)	Amalfi *et al.* (2016)
Water	-	-	Martin (1996)	Martin (1996)

2.3 Expansion valve model and additional components of the system

Charge Calculator considers the expansion device as an ideal component, in which a constant enthalpy expansion process occurs. This component does not retain any refrigerant charge.

The software, *Charge Calculator*, is able to evaluate the charge also in the additional components of the system as piping, receivers, accumulators, filters etc; for each of them, the internal volume must be provided as input. The refrigerant charge is calculated with equation (2) if the refrigerant in the additional component is single-phase or with equation (3) if the fluid is two-phase. No heat exchange and pressure drop are considered in the additional components.

2.4 System simulation

The working scheme of *Charge Calculator* is shown in Figure 1. The simulation starts by acquiring the input data:

- evaporator capacity Q_{evap}
- inlet water temperature $T_{w,in}$
- water mass flow rate $\dot{m}_w$
- inlet air dry bulb temperature $T_{a,in}$
- air mass flow rate $\dot{m}_a$
- degree of refrigerant subcooling at condenser outlet DT_{sc}
- degree of refrigerant superheating at evaporator outlet DT_{sh}
- geometrical data

The program iteratively calculates the saturation temperatures at the condenser inlet ($T_{cond,in}$), at the evaporator inlet ($T_{vap,in}$), at the evaporator outlet ($T_{vap,out}$) and the compressor frequency (f_{compr}). The iterative schemes use the secant method. The calculation procedure solves one by one the component models updating the iterative parameters. In the condenser model, the iterations on the refrigerant temperature stops when the difference between the input subcooling (DT_{sc}) and the calculated subcooling (dt_{sc}) is lower than 0.005 K. A similar criterion is used for the evaporation temperature ($T_{vap,in}$), using vapor superheating values instead of subcooling. For saturation temperature at the evaporator outlet ($T_{vap,out}$), the stopping criterion considers the difference between the values calculated in the two successive iterations; the stopping value is set equal to 0.05 K. The iterative scheme for the compressor frequency (f_{compr}) reaches convergence when the relative deviation between the calculated (q_{evap}) and input (Q_{evap}) cooling capacity is lower than 0.001. Once the iterative schemes are solved, the program calculates the charge retained by all the components considered in the simulation.

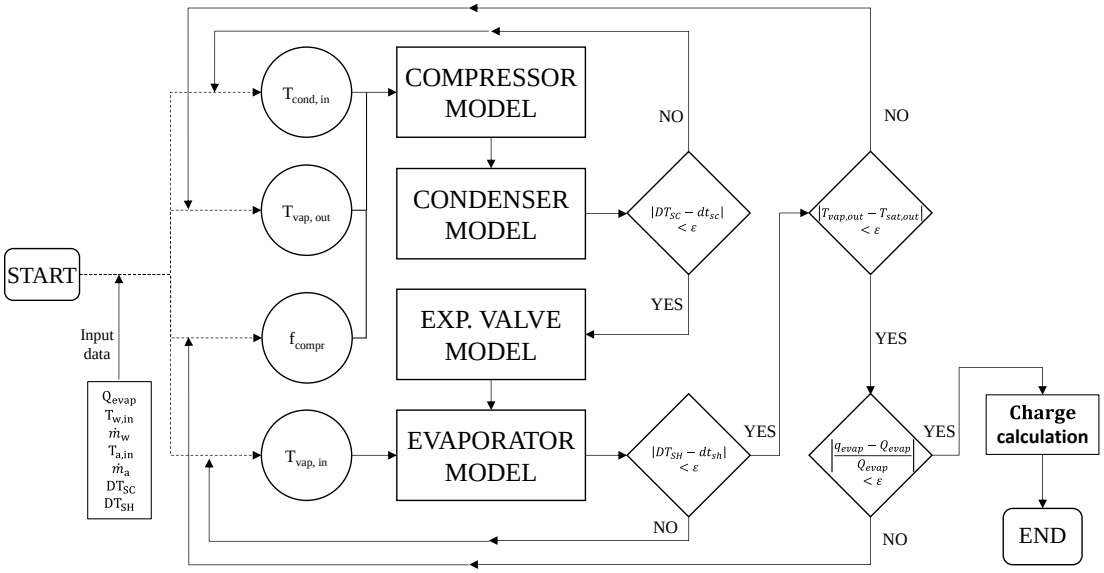

Figure 1: Working scheme of *Charge Calculator*

3. MODEL VALIDATION

The model has been validated by testing a commercialized air-to-water heat pump during cooling mode operation. The selected unit works with the refrigerant R32 and it is designed for a nominal cooling capacity of 60 kW; the refrigerant loop is shown in Figure 2. When the system works as a chiller, it produces refrigerated water at the evaporator that is a brazed plate heat exchanger with refrigerant and water flowing in counter current configuration. The unit works with two inverter driven rotary compressors, followed by an oil separator. The condenser is composed

by two fin-and-coil heat exchangers that work in parallel; the coils are internally microfinned. An electronic valve allows to expand the fluid and to control the vapor superheating at the evaporator outlet; two receivers are inserted into the circuit: a liquid receiver between the expansion device and the evaporator, and a suction accumulator prior to the compressors.

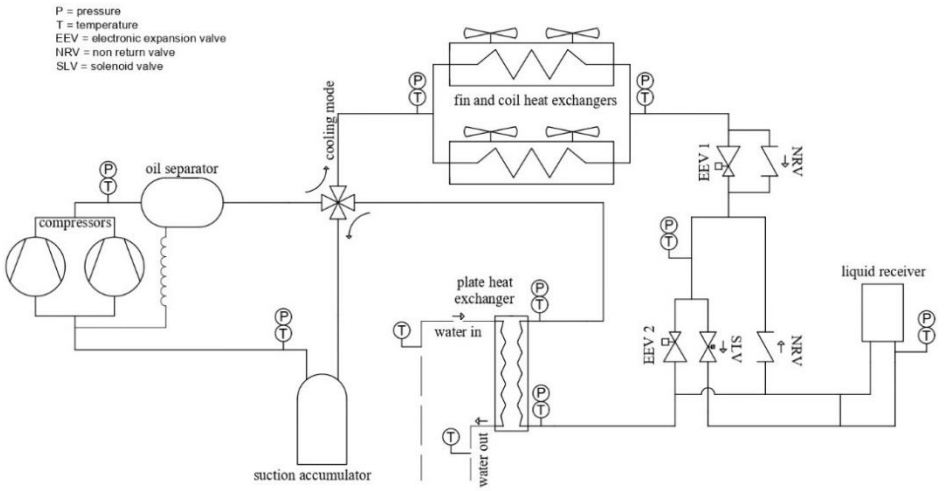

Figure 2: Refrigerant loop

The unit has been charged with 14 kg of refrigerant and tested in a climatic chamber. Refrigerant pressure and temperature are measured at the inlet and outlet of the main components: temperature is measured by means of T-type thermocouples, fixed on the external surface of the components and insulated; pressure is measured by relative pressure transducers. The water flow rate is measured using a volumetric flow meter; two platinum resistance thermometers (PRTs), inserted into the water flow, measure the inlet and outlet water temperatures. The inlet air dry bulb temperature is measured by four PRTs, equally spaced along the coil length; the accuracy for sensors and meters is reported in Table 2. The refrigerant mass flow rate circulating in the system is calculated from an enthalpy balance at the evaporator as reported in equation (4):

$$\dot{m}_r = \frac{\dot{m}_w \cdot \overline{Cp}_w \cdot \left(T_{w,in} - T_{w,out}\right)}{h_{r,out} - h_{r,in}} \tag{4}$$

where $h_{r,out}$ and $h_{r,in}$ are the refrigerant specific enthalpies at the evaporator outlet and inlet respectively. $h_{r,out}$ is calculated from the measured values of pressure and temperature at the outlet of the evaporator while $h_{r,in}$ is calculated from the values of pressure and temperature at the outlet of the condenser, considering isenthalpic the throttling process through the expansion valve.

The test conditions are reported in Table 3; they have also been imposed as input values in *Charge Calculator*. Table 4 reports the deviations between experimental and simulated results; the experimental uncertainty is also reported. The ΔT listed in Table 4 have been calculated according to equation (5):

$$\Delta T_{cond} = T_{cond,in} - T_{a,in} \qquad \Delta T_{evap} = T_w - T_{vap,out} \tag{5}$$

where $T_{cond,in}$ and $T_{vap,out}$ are the refrigerant saturation temperature at the condenser inlet and evaporator outlet respectively, $T_{a,in}$ is the inlet air dry bulb temperature, T_w is the average water temperature between inlet and outlet of the heat exchanger. The total charge predicted by the model is slightly underpredicted with a deviation from the experimental value of -9.3%. Such charge difference, equal to 1.3 kg, has been imposed as constant offset in the following simulations.

Table 2: Accuracy for sensors and instruments.

Instrument/Sensor	**Accuracy**
Refrigerant thermocouples	±0.5 °C
Pressure transducers	±1 %
Water PRTs	±0.15 °C
Water volumetric flow meter	±1 %
Air PRTs	±0.2 °C

Table 3: Test conditions.

Inlet water temperature	12 °C
Outlet water temperature	7 °C
Inlet air dry bulb temperature	35 °C
Water mass flow rate	2.45 kg s^{-1}
Air mass flow rate	10.24 kg s^{-1}
Compressor frequency	80 Hz

Table 4: Experimental vs calculated refrigerant parameters.

Parameter	Experimental	Calculated	Deviation
ΔT condenser [°C]	14.0	16.9	20.8%
ΔT evaporator [°C]	5.0	5.4	6.4%
Ref. mass flow rate [kg s^{-1}]	0.212±4.2%	0.222	4.5%
Evaporator capacity [kW]	52.44±4.2%	52.41	-0.06%
Condenser capacity [kW]	62.49±4.2%	64.61	3.4%
Compressor power [kW]	10.79±4.6%	12.20	13.0%
Refrigerant charge [kg]	14.00±0.07%	12.70	-9.3%

Table 5: Input parameters for simulations.

Parameter	Value
Water mass flow rate [kg s^{-1}]	2.86
Water inlet temperature [°C]	12
Air mass flow rate [kg s^{-1}]	10.24
Air inlet dry bulb temperature [°C]	35
Evaporator capacity [kW]	60
Refrigerant superheating [K]	7, 9, 11
Refrigerant subcooling [K]	0.5 ÷ 27.5

4. SIMULATION RESULTS

The heat pump described in the previous section has been simulated to study the effect of the refrigerant charge on the system performance and on the mass distribution. Simulations have been carried out by keeping constant all the input data required by the model and by changing the refrigerant subcooling at the condenser outlet. The input parameters for simulations are reported in Table 5.

4.1 Effect of refrigerant charge on mass distribution

Once the vapor superheating at the evaporator outlet has been fixed, the minimum theoretical refrigerant charge that guarantees stable operations for a system is the one that ensures saturated liquid at the condenser outlet; the expansion valves for sub-critical cycles, in fact, require liquid refrigerant as input for a correct operation. The extra amount of refrigerant charged into the unit is not equally distributed among the components of the system. Figure 3 shows the extra charge distribution within the unit: by adding charge to the system, most of the mass added (about the 90%), is stored inside the condenser, while the remaining 10% is distributed among the other components. Figure 4 shows the distribution of the refrigerant within the equipment as a function of the total refrigerant charge. In general, the mass increases in all the components, with the condenser that exhibits the highest increment; differently, the mass into the compressor decreases with the total charge: this is due to a lower refrigerant-oil solubility caused by an increase of the mean refrigerant and oil temperatures inside the compressor.

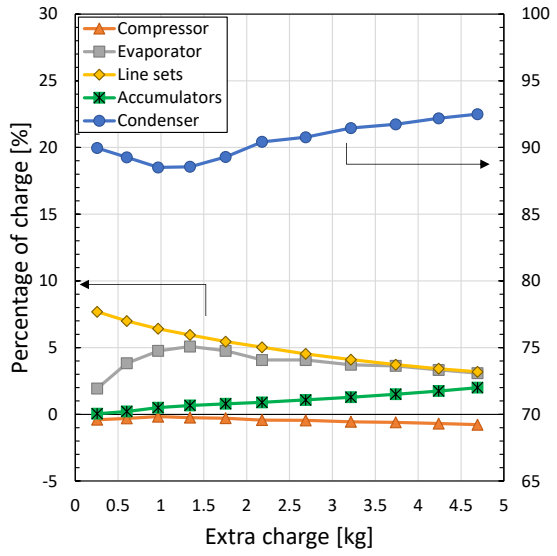

Figure 3: Distribution of extra charge (needed for subcooling) among the components of the system; the vapor superheating is set to 7 K.

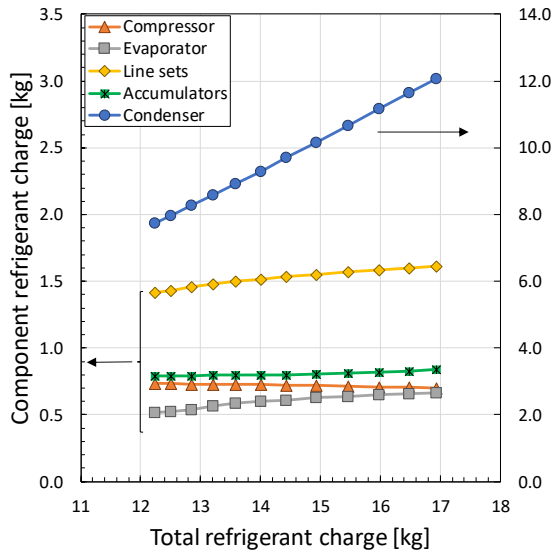

Figure 4: Distribution of refrigerant charge among the components of the system; the vapor superheating is set to 7 K.

4.2 Effect of the refrigerant charge on system performance

Figure 5 (a)-(d) shows the effect of the refrigerant charge on the system performance. Figure 5 (a) highlights the existence of a clear value of refrigerant charge, named *optimum charge*, that maximizes the system COP; by increasing the degree of vapor superheating, the optimum charge decreases, but the system COP is penalized. A similar result has been also reported by Corberán *et al.* (2008). They indicated that, when the degree of vapor superheating is increased, a greater portion of the evaporator is dedicated to produce superheated vapor, reducing the area available for evaporation and therefore the evaporation temperature. Figure 5 (b) shows the trend of pressure ratio as a function of refrigerant charge: for the lowest values of charge, the pressure ratio is almost constant, while, by increasing the charge, the increment became sharp. In fact, as shown in Figure 3, when mass is added to the system, most of it is stored into the condenser, mainly as subcooled liquid; as the degree of subcooling increases, a lower heat transfer area is available for condensation and then the condensation temperature has to increase to reject the heat absorbed. Figure 5 (c) shows the trend of refrigerant mass flow rate as a function of refrigerant charge: as pointed out, an increment in the refrigerant charge produces a higher subcooling and hence a larger refrigerating effect; since the evaporator capacity is fixed, a lower refrigerant mass flow rate is required. Two opposite effects arise when mass is added to the system: from one hand, the lower mass flow rate required allows the compressor to work at lower rotational speeds; from the other hand, the increment in pressure ratio increases the power required by the compressor. Figure 5 (d) highlights the existence of a minimum value of the compressor power in correspondence to the optimum charge.

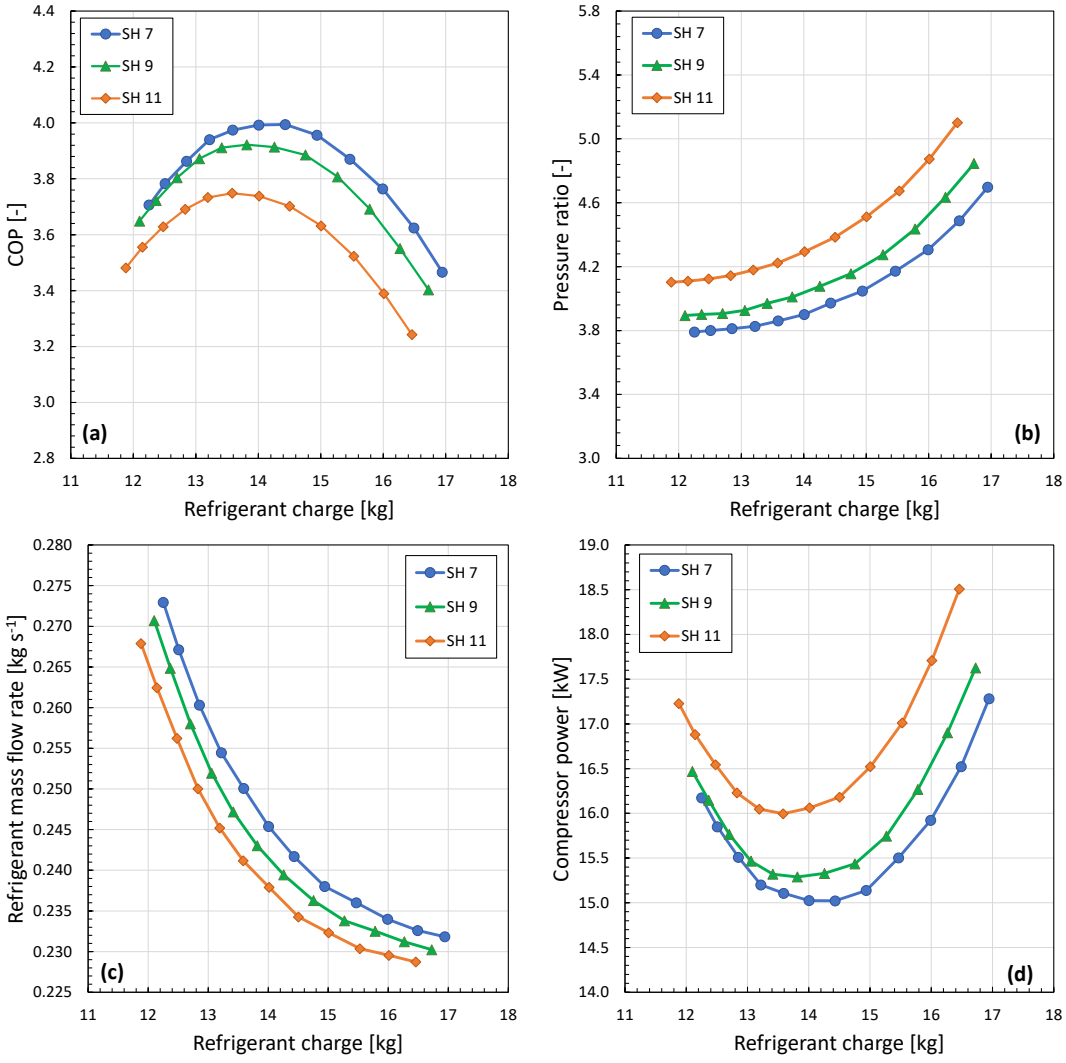

Figure 5: Effect of refrigerant charge on system performance. SH is the vapor superheating in [K].

4.3 Assessment of low-GWP refrigerants for comfort applications

The selection process of new alternative refrigerants requires an accurate analysis, which has to consider the overall environmental impact of the new equipment compared to the previous one. This section is an attempt to assess the substitution of refrigerant R32, which has a GWP_{100} equal to 675, with two low-GWP alternatives: R1234ze(E) and R290 (propane). R1234ze(E) is a mildly flammable (A2L) HFO fluid, with a GWP_{100} lower than 1 (Myhre *et al.*, 2013); R290 is a flammable (A3) natural fluid with a GWP_{100} equal to 3. Starting from the R32 system described in Section 3, two new units have been studied to produce the same cooling capacity (60 kW), one with the refrigerant R1234ze(E) and the other with R290. Regarding the new units, it is desirable that they operate with the same temperature differences in the heat exchangers and thus with the same saturation temperatures at the compressor inlet and outlet as in the R32 system. However, to reach this objective, the heat transfer area of condensers and evaporators must be increased both in the case of R290 and R1234ze(E) systems as compared to the R32 unit. However, since higher heat transfer area means higher investment cost and higher refrigerant-side volume, in the present study we did set a limit to 30% for the increase of heat transfer area both at the condenser and at the evaporator. When the maximum possible variation of heat transfer area is reached, the saturation temperatures is determined to fulfil the requirement of producing the same cooling capacity as in the R32 system. For the R1234ze(E) and R290 units, two pistons type compressors, available in the market, have been chosen and their isentropic efficiency, calculated using the manufacturers data, is reported in Table 6. The isentropic efficiency of these two piston compressors results to be lower than that of the scroll compressor used in the R32 unit.

The three systems have been simulated using *Charge Calculator*, imposing the conditions reported in Table 5 setting the vapor superheating to 7 K and the liquid subcooling to 5 K. The R1234ze(E) system would require a variation of the heat transfer area equal to 48% for the condenser and 103% for the evaporator to achieve the same saturation temperatures at the compressors inlet/outlet of the R32 unit. In this case, taking the maximum allowed variation of the heat transfer area equal to 30%, the saturation temperatures at the condenser inlet and evaporator outlet have been calculated equal to 55.8 °C and equal to 1.6 °C, respectively. For the R290 system, the heat transfer area at the condenser has been incremented by 6% and by 30% for the evaporator. The simulation results have been reported in Table 6 and the refrigerant distribution in Figure 6.

The results show that the R32 system works with the highest COP, mainly due to a better compression isentropic efficiency; on the contrary, the R1234ze(E) unit operates with the lowest COP, penalized by a lower compression isentropic efficiency and by the different saturation temperatures despite the increment in the heat transfer area. Regarding the refrigerant charge, the R1234ze(E) unit requires the highest value of charge (about 128% higher than R32 system) to produce the same useful effect, while the propane equipment requires a charge reduction equal to 44% compared to the R32 system. The differences lie both on the different internal volumes of the three systems and on the different densities of the refrigerants.

In order to evaluate which of the three systems exhibit the lowest environmental impact, the TEWI index has been calculated. TEWI is a parameter that combines both direct and indirect effects of a system; it represents the tons of equivalent CO_2 released into the atmosphere during the whole lifetime of the equipment.

The value of TEWI is calculated using equation (6):

$$TEWI = X \cdot GWP + \beta \cdot P_{compr} \cdot H \cdot n \tag{6}$$

where X is the total amount of refrigerant released into the atmosphere during the whole lifetime of the equipment, β is the emission rate, H is the number of operating hours per year of the unit, n is the system lifetime. The values used for this analysis have been extracted from Sand *et al.* (1997) and reported in Table 7.

Table 6: Simulation results for the R32, R1234ze(E) and R290 systems.

	R32	**R1234ze(E)**	**R290**
Condensation temperature [°C]	54.77	55.82	54.81
Condenser pressure drop [bar]	0.27	0.12	0.26
Evaporation temperature [°C]	3.48	1.58	3.53
Evaporator pressure drop [bar]	0.14	0.23	0.12
Pressure ratio [-]	3.86	5.03	3.60
Refrigerant mass flow rate [kg s^{-1}]	0.26	0.49	0.23
Compression isentropic efficiency [-]	0.73	0.68	0.68
COP [-]	2.90	2.64	2.81

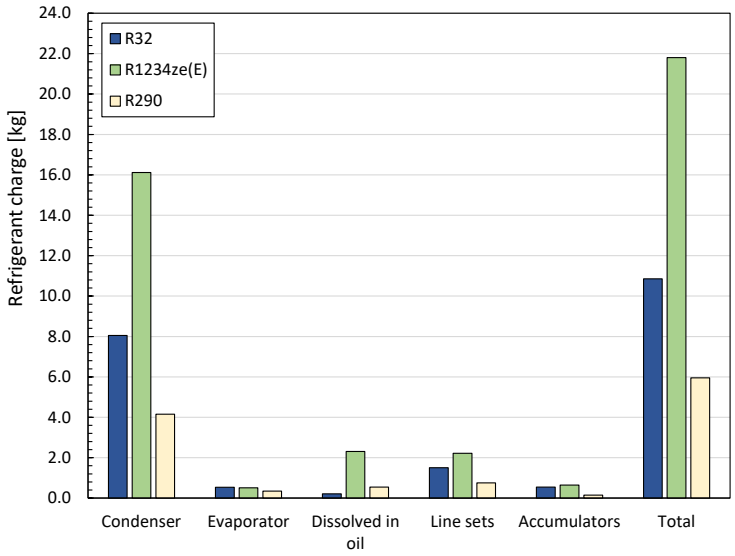

Figure 6: Refrigerant distribution for the R32, R1234ze(E) and R290 systems.

In the study we consider an annual loss rate equal to 2% of the total charge and an end-of-life loss rate equal to 5% of the total charge. Table 8 reports the results: the lowest indirect effect is generated by the R32 system, which has the highest COP. Regarding the direct effect, the systems with propane and R1234ze(E) exhibit low values of direct TEWI; the direct TEWI contributes for a fraction lower than 3% of the total TEWI. To conclude, the unit with R32 and R290 present lower environmental impacts.

Table 7: Parameters used for the TEWI analysis.

Parameter	**Value**
Emission rate[1] (Italy value)	0.29 kg kWh^{-1}
Annual operating rate (full-load hours)	2125 h $year^{-1}$
Equipment lifetime	30 years
Annual loss rate	2% of the total charge
End-of-life loss rate	5% of the total charge

[1] value for the year 2019, calculated by ISPRA (2019)

Table 8: Direct, Indirect and Total TEWI for the R32, R1234ze(E) and R290 systems.

Refrigerant	**GWP_{100} [-]**	**Indirect TEWI [ton $CO_{2,eq}$]**	**Direct TEWI [ton $CO_{2,eq}$]**	**Total TEWI [ton $CO_{2,eq}$]**
R32	675	382.739	4.762	387.501
R1234ze(E)	1	419.257	0.014	419.271
R290	3	395.022	0.012	395.034

6. CONCLUSIONS

A model for the performance simulation of air-to-water systems has been described and validated in this paper; the model is able to predict the refrigerant mass distribution among the components of the system. An air-to-water equipment has been selected as a case study to analyse the influence of the refrigerant charge on mass distribution and system performance during the cooling mode operations. The unit selected is a reversible heat pump, which works with refrigerant R32 and produces a nominal cooling capacity of 60 kW. The results of the simulations have shown, as expected, that the highest fraction of charge is stored within the condenser; the simulations highlighted the existence of a clear value of charge that maximize the system COP. In the attempt to assess long-term alternative to the refrigerant R32, two new equipment, one working with the R1234ze(E) and the other with propane (R290) have been

simulated. The requirement is that the three units have to produce the same cooling capacity, possibly with the same saturation temperature of the R32 unit, but allowing a heat transfer area increase up to 30% both in the condenser and in the evaporator. In the case of the unit working with R1234ze(E), even with an increment of the heat transfer area equal to 30% at condenser and evaporator, to produce the same cooling capacity of the R32 system it is necessary to increase the condensing temperature and decrease the evaporation temperature, thus penalizing the COP. The results of the simulations showed that the R32 system exhibits the highest COP and the lowest value of indirect TEWI. The system with R290, even if it results to have a lower COP (compared to the R32 unit), presents a TEWI comparable with that of R32.

NOMENCLATURE

COP	Coefficient of performance	(-)
Cp	Specific heat at constant pressure	(J kg^{-1} K^{-1})
dt, DT	Temperature difference	(K)
f	Compressor frequency	(Hz)
h	Specific enthalpy	(J kg^{-1})
H	Operating hours per year of the unit	(h $year^{-1}$)
$\dot{m}$	Mass flow rate	(kg s^{-1})
M	Mass	(kg)
n	system lifetime	(years)
P	power	(W)
q, Q	Thermal capacity	(W)
T	Temperature	(°C)
$T_{cond, in}$	Saturated temperature at condenser inlet	(°C)
$T_{vap, in}$	Saturated temperature at evaporator inlet	(°C)
$T_{vap, out}$	Saturated temperature at evaporator outlet	(°C)
V	Volume	(m^3)
X	Amount of refrigerant released in atmosphere	(kg)

Greek

α	Void fraction	(-)
β	Emission rate	(kg kWh^{-1})
ε	Error	(-)
ξ	Refrigerant-oil solubility	(-)
ρ	Density	(kg m^{-3})

Subscript

a	air
compr	compressor
evap	evaporator
in	inlet
l	liquid
r	refrigerant
sc	subcooling
sh	superheating
v	vapor
w	water

REFERENCES

Abu Madi, M., Johns, R. A., & Heikal, M. R. (1998). Performance Characteristics Correlation for Round Tube and Plate Finned Heat Exchangers. *International journal of refrigeration* 21(7): 507–17.

Amalfi, R. L., Vakili-Farahani, F., & Thome, J. R. (2016). Flow Boiling and Frictional Pressure Gradients in Plate Heat Exchangers. Part 2: Comparison of Literature Methods to Database and New Prediction Methods. *International Journal of Refrigeration* 61: 185–203.

Baroczy, C. J. (1963). Correlation of Liquid Fraction in Two-Phase Flow with Application to Liquid Metals. *Atomics International*.

Cavallini, A., Del Col, D., Mancin, S., & Rossetto, L. (2009). Condensation of Pure and Near-Azeotropic Refrigerants in Microfin Tubes: A New Computational Procedure. *International Journal of Refrigeration* 32(1): 162–74.

Corberán, J. M. (2010). Role, Sizing and Influence of the Liquid Receiver. *IIR 2nd Workshop on Refrigerant Charge Reduction*.

Corberán, J. M., Martínez, I. O., & Gonzálvez, J. (2008). Charge Optimisation Study of a Reversible Water-to-Water Propane Heat Pump. *International Journal of Refrigeration* 31(4): 716–26.

Istituto Superiore per la Protezione e la Ricerca Ambientale (ISPRA). (2019). Fattori emissione produzione e consumo elettricità_2019. http://www.sinanet.isprambiente.it/it/sia-ispra/serie-storiche-emissioni/fattori-di-emissione-per-la-produzione-ed-il-consumo-di-energia-elettrica-in-italia/view, last access: January 22, 2021.

Lemmon, E. W., Huber, M. L., & McLinden, M. O. (2013). NIST Standard Reference Database 23, NIST Reference Fluid Thermodynamic and Transport Properties, REFPROP, Version 9.1. *Standard Reference Data Program*.

Li, G. Q., Wu, Z., Li, W., Wang, Z. K., Wang, X., Li, H. X., & Yao, S. C. (2012). Experimental Investigation of Condensation in Micro-Fin Tubes of Different Geometries. *Experimental thermal and fluid science* 37: 19–28.

Martin, H. (1996). A Theoretical Approach to Predict the Performance of Chevron-Type Plate Heat Exchangers. *Chemical Engineering and Processing: Process Intensification* 35(4): 301–10.

Myhre, G. et al. (2013). Anthropogenic and Natural Radiative Forcing. Climate Change 2013: The Physical Science Basis. Contribution of Working Group I to the Fifth Assessment Report of the Intergovernmental Panel on Climate Change, 659–740.

Navarro, E., Corberán, J. M., Martínez-Galvan, I. O., & Gonzalvez, J. (2012). Oil Sump Temperature in Hermetic Compressors for Heat Pump Applications. *International journal of refrigeration* 35(2): 397–406.

Ravigururajan, T. S., & Bergles, A. E. (1996). Development and Verification of General Correlations for Pressure Drop and Heat Transfer in Single-Phase Turbulent Flow in Enhanced Tubes. *Experimental Thermal and Fluid Science* 13(1): 55–70.

Regulation, E U. 2014. No 517/2014 of the European Parliament and the Council of 16 April 2014 on Fluorinated Greenhouse Gases and Repealing Regulation (EC) No 842/2006. *J. Eur. Union* 57: 195–230.

Sand, J. R., Fischer, S. K., & Baxter, V. D. (1997). Energy and Global Warming Impacts of HFC Refrigerants and Emerging Technologies. Citeseer.

Taitel, Y., & Barnea, D. (1990). Two-Phase Slug Flow. *Advances in Heat Transfer*, Elsevier, 83–132.

ACKNOWLEDGEMENT

The authors gratefully acknowledge the company Clivet S.p.A. for the financial support to this research.